Journal of Alloys and Compounds 508 (2010) 540–545

Contents lists available at ScienceDirect

Journal of Alloys and Compounds

journal homepage: www.elsevier.com/locate/jallcom

Microstructure and mechanical properties of TiN/Si_3N_4 nanocomposites by spark plasma sintering (SPS)

Ching-Huan Lee[a], Horng-Hwa Lu[b], Chang-An Wang[c], Pramoda K. Nayak[a], Jow-Lay Huang[a,*]

[a] Department of Materials Science and Engineering, National Cheng-Kung University, Tainan 701, Taiwan, ROC
[b] Department of Mechanical Engineering, National Chin-Yi University of Technology, Taiping, Taichung 411, Taiwan, ROC
[c] State Key Lab of New Ceramics and Fine Processing, Department of Materials Science and Engineering, Tsinghua University, Beijing 100084, People's Republic of China

ARTICLE INFO

Article history:
Received 9 June 2010
Received in revised form 24 August 2010
Accepted 25 August 2010
Available online 28 September 2010

Keywords:
Sintering
Nanocomposites
Electrical properties
Mechanical properties
Si_3N_4

ABSTRACT

TiN/Si_3N_4 nanocomposites were fabricated from β-Si_3N_4 and TiN nano powders by powder processing routes. The specimens were consolidated at 1600 °C for 3 min by spark plasma sintering, and nearly full densification was obtained in the resulting sintered bulk composites. The TiN phase grows rapidly and a typical twin structure of TiN can be observed in the composites. The grain size and distribution for TiN may affect the electrical resistivity, leading to a pulse current through the sintering compact. The resulting microstructure for the composite containing 10 wt% TiN reveals that grain coarsening behavior for β-Si_3N_4 based grains is accelerated, and the composite has the highest toughness of 4.9 MPa $m^{1/2}$ among all these composites. The other composites show nanosized β-Si_3N_4 based grains with a fracture toughness of nearly 4.2 MPa $m^{1/2}$.

1. Introduction

Silicon-based non-oxide ceramics have attracted much attention, primarily due to their good mechanical and chemical properties, and also their reliablity at room and elevated temperatures [1,2]. They have great potential for two industrial uses, as engineering components and cutting-tool applications. Specially, ceramic-reinforced Si_3N_4 is known as one of the materials with the most potential for high-temperature structural applications.

TiN is often incorporated into the β-Si_3N_4 matrix as cutting-tool materials [1,3–5]. There are two advantages to the Si_3N_4 based composites. First of all, the good physical properties of TiN, such as high melting point, hardness, strength and chemical stability, as well as its good erosion and corrosion resistance, enable it to be an excellent toughening material [5–7]. Secondly, the electrical resistance of Si_3N_4 can be substantially decreased, which consequently makes electric-discharge machining (EDM) possible [1,8,9].

Spark plasma sintering is a newly developed sintering technique, which is beneficial to consolidating Si_3N_4 based nanocomposites in a short time. The present authors have reported that TiN/Si_3N_4 based nanocomposites with excellent mechanical properties and conductivity can be processed through a chemical route and sintered by SPS [10,11]. However, due to the complexity of these processing techniques, they are not suitable for large-scale production. The planetary milling process is introduced in this study. Moreover, the microstructural development of Si_3N_4 and TiN was not described in detail previously, especially in the presence of a pulse direct current through the sintering compact during a sintering cycle. The Si_3N_4 and TiN nano powders were applied because they are sensitive to the microstructural changes during the sintering process. The relationship between microstructure and performance, like mechanical properties and electrical conductivity, of these TiN/Si_3N_4 nanocomposites are discussed in the present study.

2. Experimental procedure

The raw material used in this study is a commercially available Si_3N_4 nano powder (SM131, Fraunhofer-Institut für Keramische Technologien and Sinterwerkstoffe, Dresden, Germany) doped with sintering additives of 6 wt% Y_2O_3 and 8 wt% Al_2O_3. It contains 90 wt% β-phase and 10 wt% α-phase, with a manufacturer-determined average particle size of 70 nm by the Rietveld method. Nanosized TiN with size of ~30 nm (Hefei Kiln Nanometer Technology Development, Hefei, China) was mixed with Si_3N_4 nano powders. The composition was chosen to yield a TiN content of 5, 10, 15, 20, and 30 wt% in the final product. The specimen designations and corresponding TiN/Si_3N_4 ratios in volume percentage (vol.%) for each composite are shown in Table 1. The mixing powders were ultrasonically dispersed in ethanol for 15 min, and then mixed by planetary milling at a rotation speed of 300 rpm for 6 h using a 375 ml nylon bottle with Si_3N_4 balls. The powder mixture was dried in a rotary evaporator, cold-iso-statically pressed into round ingots at a pressure of 200 MPa, crushed and then passed through a #200 sieve for granulation.

The granulated powders were loaded in a cylindrical carbon die with an inner diameter of 20 mm for SPS (Dr. Sinter 1050, Sumitomo Coal Mining, Kawasaki, Japan). The SPS experiments were carried out at 1600 °C with a 3 min dwell time

* Corresponding author. Tel.: +886 6 2348188; fax: +886 6 2763586.
E-mail address: JLH888@mail.ncku.edu.tw (J.-L. Huang).

0925-8388/$ – see front matter © 2010 Elsevier B.V. All rights reserved.
doi:10.1016/j.jallcom.2010.08.116

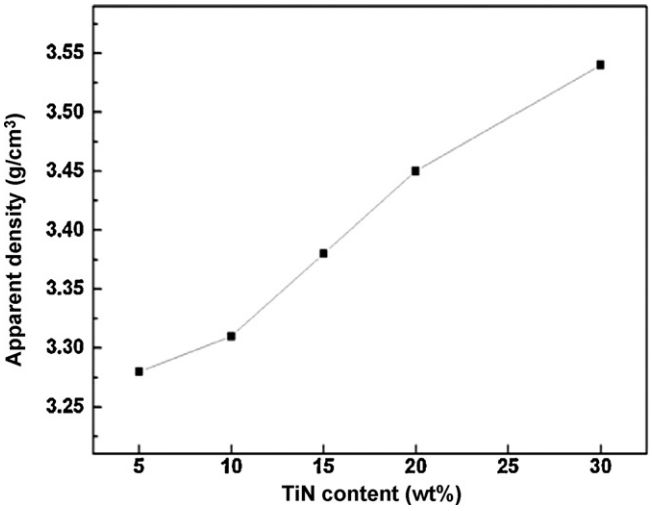

Fig. 1. Change of apparent density of the composites with TiN content; samples were sintered at 1600 °C for 3 min with a heating rate of 200 °C/min in a vacuum.

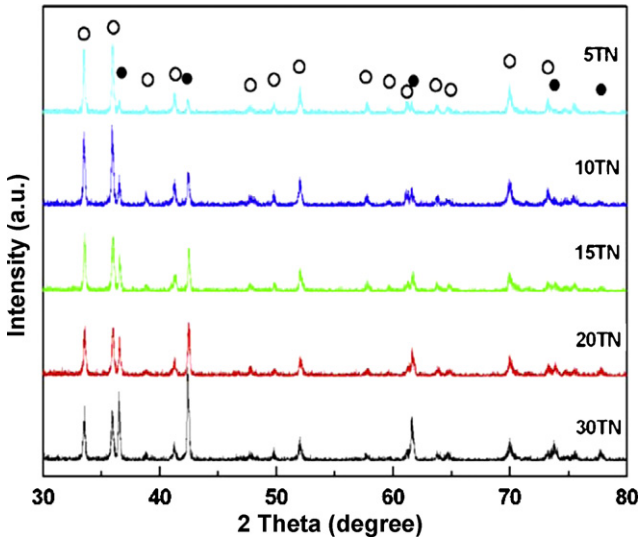

Fig. 2. X-ray diffraction patterns of composites with varying TiN content. (○) β-SiAlON, and (●) TiN; samples were sintered at 1600 °C for 3 min with a heating rate of 200 °C/min in a vacuum.

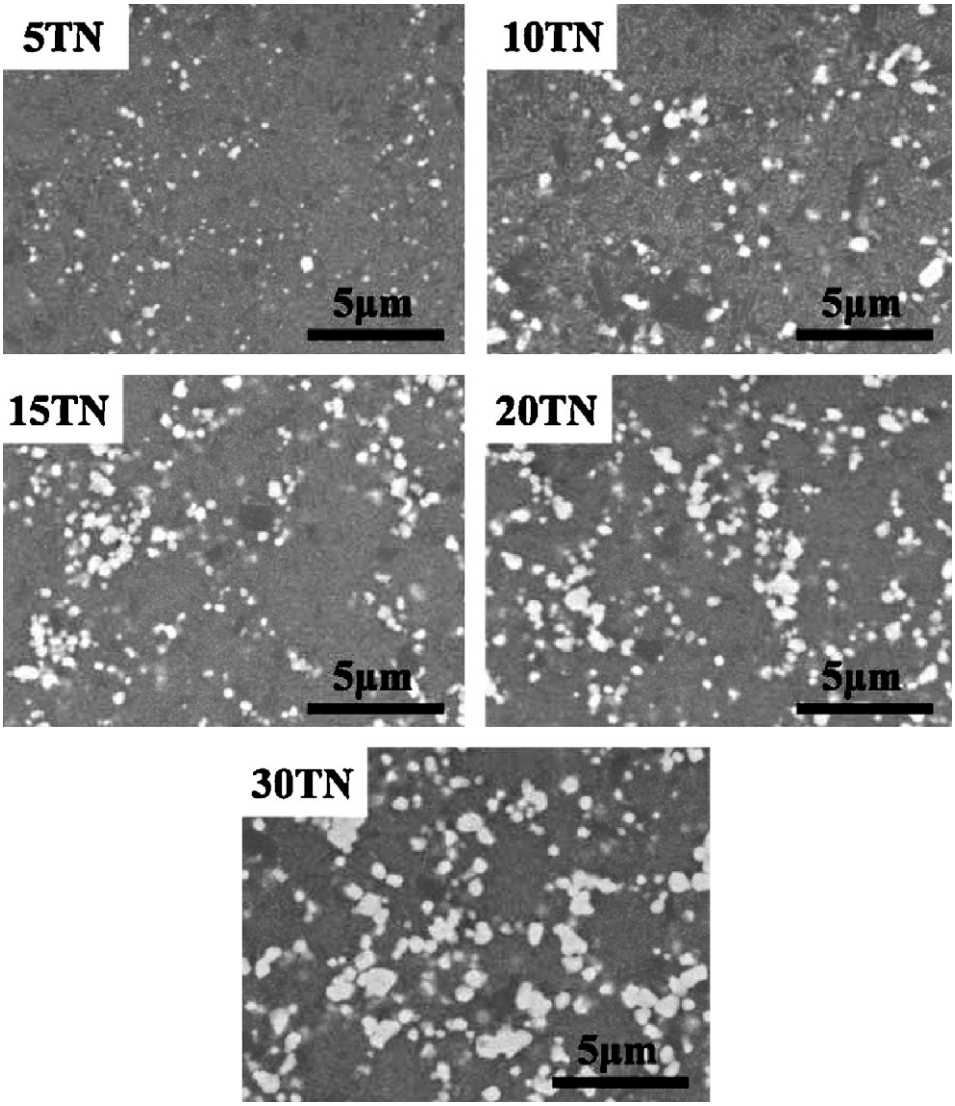

Fig. 3. Backscattered SEM images of polished TiN/Si_3N_4 composites with varying TiN content; samples were sintered at 1600 °C for 3 min with a heating rate of 200 °C/min in vacuum. The brighter phase is TiN phase and the darker phase is β-SiAlON matrix.

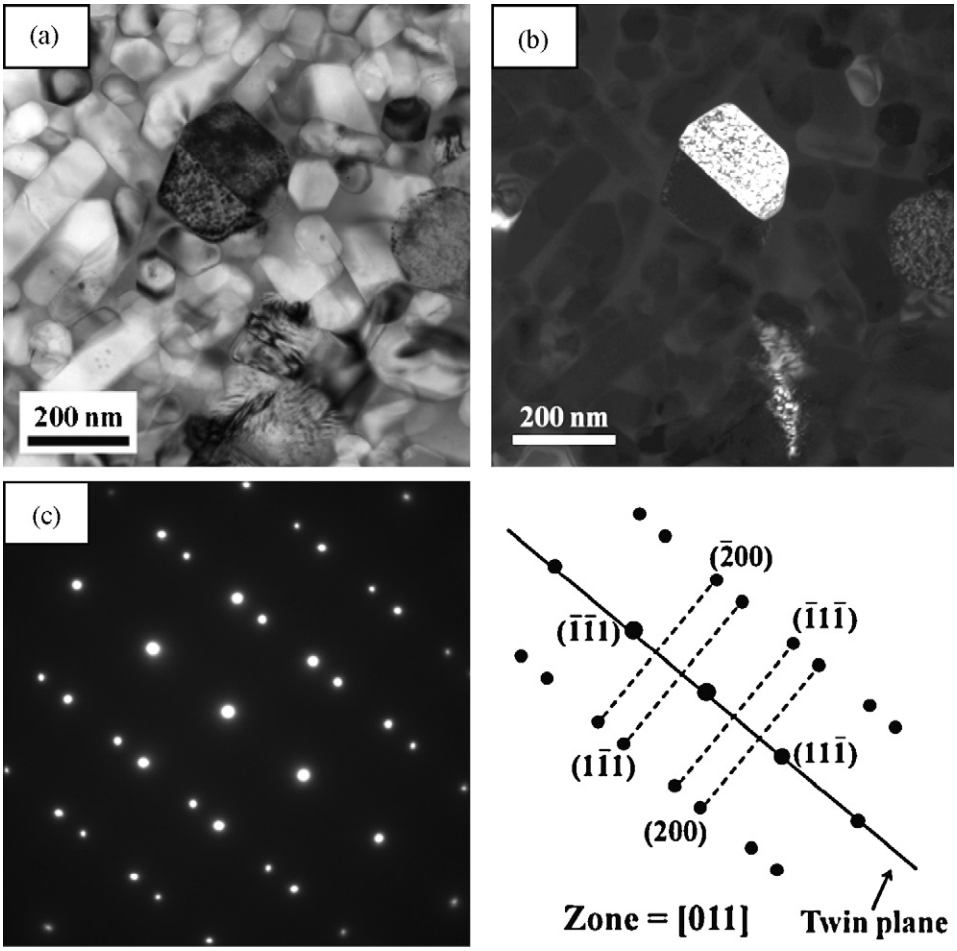

Fig. 4. (a) Bright field and (b) dark field micrographs, and (c) [0 1 1] selected area diffraction patterns of TiN in spark plasma sintered TiN/Si_3N_4 composite containing 10 wt% TiN. The existence of a twin structure is observed.

and under 30 MPa uniaxial pressure in a vacuum. The heating rate was 200 °C/min. The temperature was monitored by an optical pyrometer. The effective densities of the sintered composites were measured by the Archimedes principle. Phase identification was performed by an X-ray diffractometer (XRD; Model D-MAX/IIB, Rigaku, Tokyo, Japan). Cell dimensions were determined from XRD peak data using UNITCELL with a Si standard. A semiconductor parameter analyzer for the resistance measurements (HEWLETT PACKARD 4140B, USA) was used to determine the electrical resistivity of the samples. The upper surfaces of the sintered samples were polished down to 1 μm. Hardness was measured with a Vickers hardness tester (AKASHI AVK-A, Japan) and by applying a micro-hardness indent at 196 N for 15 s. Fracture toughness was measured by the Vickers surface indentation technique [12]. The polished and plasma etched surfaces were used for microstructural characterization by field emission scanning electron microscope (FESEM, XL-40FEG, Philips, The Netherlands). A sample prepared following the same procedure as the as-received Si_3N_4 nano powder, but without adding the TiN phase was used as a comparison (denoted as 0TN). A thin specimen was prepared with a focused ion beam system (FIB, SEIKO, SMI3050, Japan). Transmission electron microscopy (FEG-TEM, Tecnai G2 F20, Philips, Eindhoven, The Netherlands) was used to characterize the TiN grain of the sintered sample.

3. Results and discussion

Fig. 1 shows the apparent density of samples containing up to 30 wt% TiN. The apparent density was found to increase with the increase of TiN content. The increase in density is as predicted, because the theoretical density of TiN (5.39 g/cm^3) is substantially greater than that of monolithic Si_3N_4. (3.19 g/cm^3) [13]. No obvious pores were observed on the polished surfaces of the samples, which suggest the TiN/Si_3N_4 composites were near full densification.

The typical X-ray diffraction patterns of these sintered composites with varying TiN content are presented in Fig. 2. These composites consist of the β-Si_3N_4 phase as a major phase along with coexistence with the TiN phase. The intensity of TiN peaks continues to increase with increasing TiN content. The value of the lattice constant for TiN is 4.25 Å, approaching that of pure TiN. On the other hand, the values for a_0 and c_0 for the β-Si_3N_4 phase are

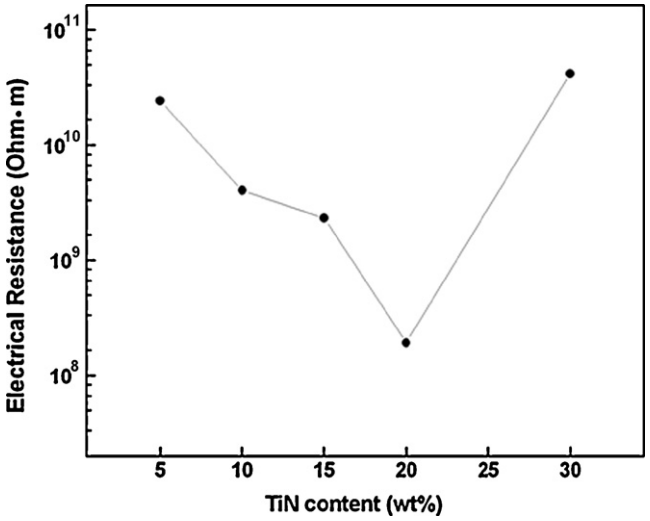

Fig. 5. Change of electrical resistance of TiN/Si_3N_4 composites with varying TiN content; samples were sintered at 1600 °C for 3 min with a heating rate of 200 °C/min in a vacuum.

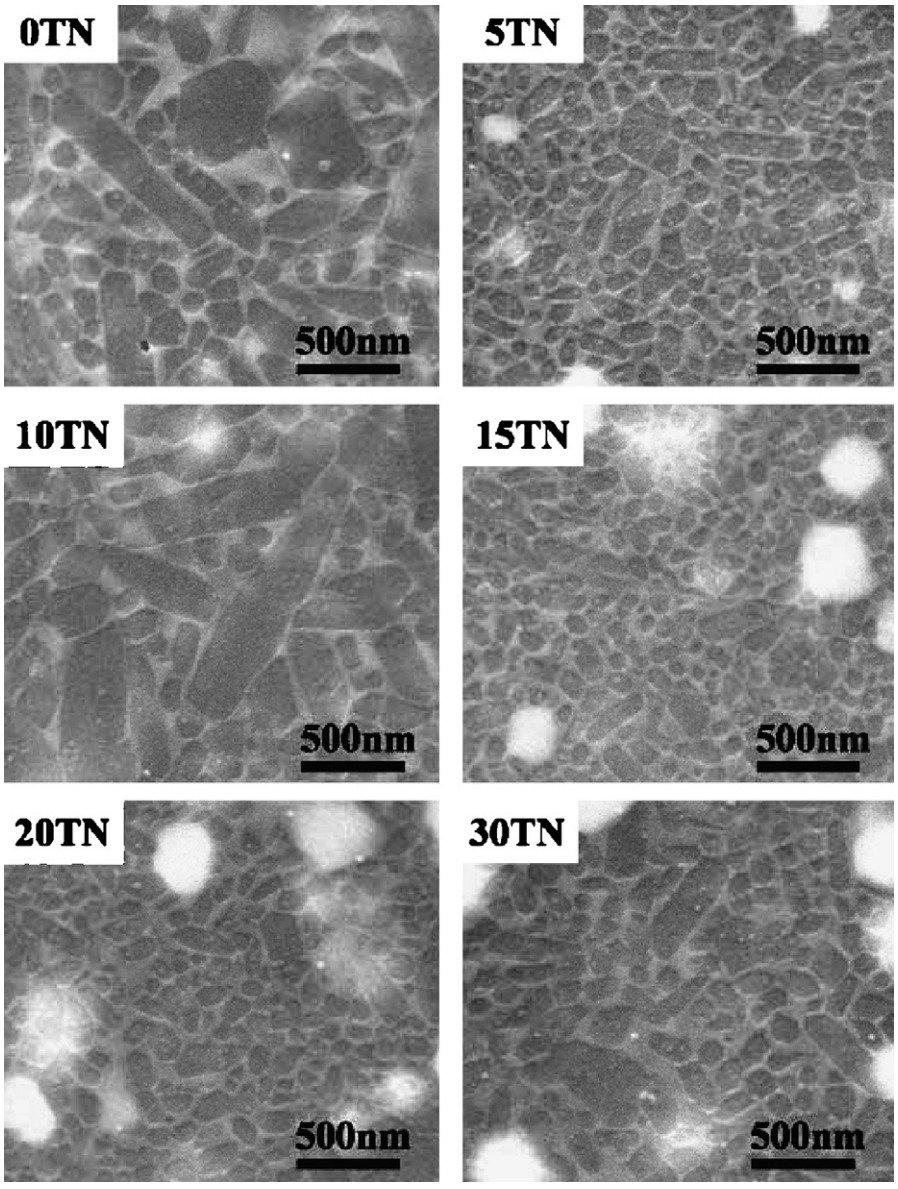

Fig. 6. SEM micrographs showing the etching surface of TiN/Si_3N_4 composites with varying TiN content; samples were sintered at 1600 °C for 3 min with a heating rate of 200 °C/min in a vacuum.

7.61 and 2.91 Å, respectively, which are somewhat deviated from those for pure β-Si_3N_4 (+0.01 Å). This result suggests that a tiny amount of Si–N may be replaced by Al–O in the particle dissolution and coarsening stages of liquid phase sintering and form the β-SiAlON phase [14].

Fig. 3 shows backscattered electron images in SEM of the polished surface of composites with varying TiN content. The samples were sintered at 1600 °C for 3 min with a heating rate of 200 °C/min in a vacuum. The lighter and heavier atoms in the backscattered images show up as the gray and white regions corresponding to the β-SiAlON matrix (including glassy phase) and TiN particles. Therefore, the TiN particles are distributed homogeneously in the β-SiAlON matrix. However, most of the TiN appear as submicro-sized grains, which are much larger than the size of the starting nano powders.

The typical bright field and dark field images of the TiN grain for the as-sintered composite containing 10 wt% TiN content sintered at 1600 °C for 3 min with a heating rate of 200 °C/min are shown in Fig. 4(a) and (b), respectively. Fig. 4(c) is the [0 1 1] selected area diffraction pattern (SAD) for the submicrosized TiN grain, and it shows the existence of a twin structure. The results suggest that grain growth and coalescence of TiN occurs in the composite during the spark plasma sintering process in a short time.

The change in electrical resistance for the composites with varying TiN content is shown in Fig. 5. The electrical resistance substantially decreases from 2.43×10^{10} (5 TN) to 1.93×10^{8} (20 TN)

Table 1
Specimen designation of composites with varying TiN content; samples were sintered at 1600 °C for 3 min with a heating rate of 200 °C/min in a vacuum.

TiN/Si_3N_4 content ratio (wt%)	5	10	15	20	30
Designation	5 TN	10 TN	15 TN	20 TN	30 TN
TiN/Si_3N_4 content ratio (vol.%)	3.31	6.75	10.06	14.00	21.81

(Ω m) with the increase in TiN content, whereas it suddenly increases to a value of 4.19×10^{10} (Ω m) for composite 30 TN. It has been reported that if the fraction of conductive TiN phase in the composite is under the degree of percolation threshold, the insulating property of the composites is maintained as the electrical resistance of non-conductive Si_3N_4 matrix [15]. This suggests the TiN phase does not form a connective network. As it is evidenced from Fig. 3, the submicrosized TiN grains are nearly isolated from each other. Moreover, the change of electrical resistance possibly depends on the grain size of the conductive phase [16]. Compared with the special cases for 20 TN and 30 TN, the larger particle size of TiN for 30 TN increases the interparticle distance, leading to a higher magnitude of electrical resistance over composite 20 TN.

The typical micrographs of β-SiAlON grains with different TiN content are presented in Fig. 6. In general, the TiN in TiN/Si_3N_4 based composite inhibits grain boundary diffusion and reduces the grain size of the Si_3N_4 matrix [17]. However, for the special case of 10 TN among these composites, the large, elongated grains can be obtained. The conductive phase of TiN might play an important role in the microstructural development of TiN/Si_3N_4 based composites. The electrical resistivity of TiN (3.34×10^{-7} Ω m) [1] is in the range of metallic materials. Although a tiny current appears as measured by a semiconductor parameter analyzer, it is reasonable that a large current might be induced in the presence of pulsed electrical field during sintering. A leakage current might go through the sintering compact during a heating process, and a similar phenomena is also proposed in ferroelectric ceramics [18,19], and $TiC_xO_yN_z/Si_3N_4$ based nanocomposites [20]. Therefore, we can expect that a direct current might hop across conductive TiN grains embedded in the insulating β-SiAlON matrix when applying a pulse current. A temporary high temperature might occur in the specimen, and consequently accelerate the grain coarsening behavior of β-SiAlON during a sintering cycle.

Except for the case of the 10 TN composite, most of the β-SiAlON grains for the composites have an equiaxial shape with a grain size of less than 200 nm (as shown in Fig. 6), whereas a tiny amount of elongated grains with a grain width of 100 nm were observed. For the composite of 5 TN, the percolation concentration is too low (i.e. the interparticle distance of TiN is large) to allow a pulse current to pass through the sintering body [15]. For the samples of 15 TN, 20 TN, and 30 TN, the TiN phase significantly inhibits the grain growth of the β-SiAlON matrix, even though it is possible for a pulse current to pass through the samples during sintering.

The influence of the TiN content of TiN/Si_3N_4 based nanocomposites on the Vickers hardness is shown in Fig. 7. The hardness value for these composites decreases with an increasing amount of TiN phase in the β-SiAlON matrix, and a similar trend was also observed by Lee et al. [21].

The fracture toughness of the composites containing various compositions of TiN measured by the indentation technique for composites is shown in Fig. 8. The monolithic Si_3N_4 ceramics have the highest value of 5.4 MPa $m^{1/2}$. Among the TiN/Si_3N_4 composites, the toughness reaches a maximum value of 4.9 MPa $m^{1/2}$ for the composite containing 10 wt% TiN, whereas the other composites have values lower than 4.2 MPa $m^{1/2}$. An equation which expresses the increase in toughness as function of grain size, derived by Buljan et al. [22] under the assumption that the grain shapes are the same, is given by

$$dK_c = CK_c^0 \left(\frac{dD}{D_0} - 1 \right) \quad (1)$$

where C is a coefficient dependent on the mode of fracture; K_c^0 and D_0 are the initial toughness and grain size; dK_c and dD are the respective changes in toughness and diameter. Hence, the changes in grain size and shape are directly related to toughness. An increase in Si_3N_4 grain size results in increasing fracture toughness. Although the addition of TiN does not improve the mechanical properties of Si_3N_4 based composites, the special sintering behavior produced by pulse direct current (grain coarsening effect for Si_3N_4 based grain) may occur in a SPS process.

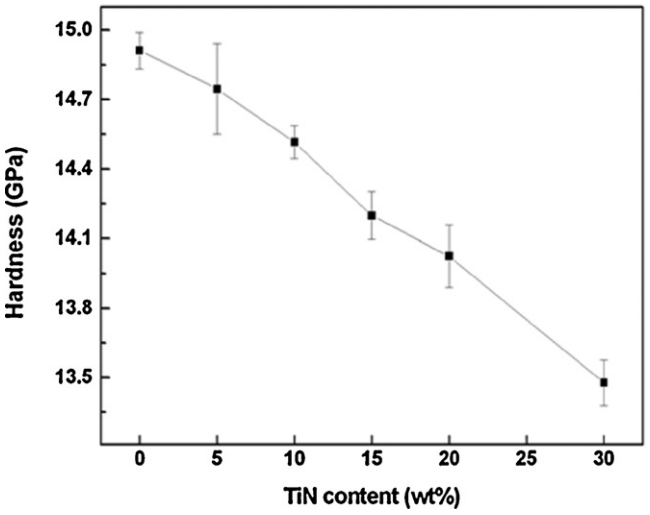

Fig. 7. Vickers hardness of TiN/Si_3N_4 composites with various TiN content; samples were sintered at 1600 °C for 3 min with a heating rate of 200 °C/min in a vacuum.

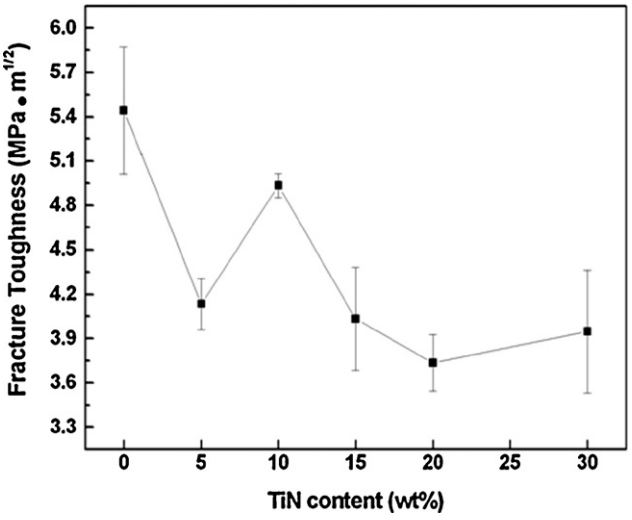

Fig. 8. Fracture toughness measured by Vickers surface indentation technique versus TiN compositions; samples were sintered at 1600 °C for 3 min with a heating rate of 200 °C/min in a vacuum.

4. Conclusions

(1) By utilizing Si_3N_4 and TiN nano powders as starting materials, a series of near-fully dense TiN/Si_3N_4 based nanocomposites containing varying TiN contents (5–30 wt%) have been fabricated successfully by a spark plasma sintering technique.
(2) A grain coalescence of the TiN phase has been demonstrated by TEM. The conductive TiN grains in the insulating Si_3N_4 matrix are observed to be isolated from each other. From the microstructural observations, the composites appear to be insulating materials.
(3) For the nanocomposite of 5 TN, 15 TN, 20 TN, and 30 TN, the TiN phase inhibits the grain growth of Si_3N_4 based grains during sintering. Hence, the nanosized Si_3N_4 based crystallites are maintained in size as the raw material.

(4) The spark plasma sintered TiN/Si_3N_4 based composite containing 10 wt% TiN achieves the largest grain size and the highest toughness of 4.9 MPa $m^{1/2}$ compared to the other composites. A possible pulse current sintering mechanism might occur, which causes a temporary high temperature in the sintering compact, and then accelerates the grain coarsening of Si_3N_4 based grains.

Acknowledgement

The authors thanks to the National Science Council of the ROC for its financial support under the contract no. NSC 99-2923-E-006-002-MY3.

References

[1] Y.G. Gogotsi, J. Mater. Sci. 29 (10) (1994) 2541–2556.
[2] J.L. Huang, S.Y. Chen, M.T. Lee, J. Mater. Res. 9 (9) (1994) 2349–2354.
[3] Z. Guo, G. Blugan, R. Kirchner, M. Reece, T. Graule, J. Kuebler, Ceram. Int. 33 (7) (2007) 1223–1229.
[4] S. Balakrishnan, J.S. Burnellgray, P.K. Datta, in: S. Hampshire, M. Buggy, B. Meenan, N. Brown (Eds.) Key Eng. Mater. 99 (1) (1995) 279–289.
[5] C.C. Liu, J.L. Huang, Ceram. Int. 29 (6) (2003) 679–687.
[6] G. Blugan, M. Hadad, J. Janczak-Rusch, J. Kuebler, T. Graule, J. Am. Ceram. Soc. 88 (4) (2005) 926–933.
[7] M. Yoshimura, O. Komura, A. Yamakawa, Scripta Mater. 44 (8–9) (2001) 1517–1521.
[8] S. Kawano, J. Takahashi, S. Shimada, J. Mater. Chem. 12 (2) (2002) 361–365.
[9] L. Gao, J.G. Li, T. Kusunose, K. Niihara, J. Eur. Ceram. Soc. 24 (2) (2004) 381–386.
[10] S. Kawano, J. Takahashi, S. Shimada, J. Am. Ceram. Soc. 86 (4) (2003) 701–705.
[11] E. Ayas, A. Kara, F. Kara, J. Ceram. Soc. Japan 116 (1355) (2008) 812–814.
[12] A.G. Evans, E.A. Charles, J. Am. Ceram. Soc. 59 (7–8) (1976) 371–372.
[13] D.R. Lide, CRC Handbook of Chemistry and Physics, 83rd ed., CRC Press, Boca Raton, 2002–2003.
[14] Z.J. Shen, M. Nygren, J. Mater. Chem. 11 (1) (2001) 204–207.
[15] L. Zivkovic, Z. Nikolic, S. Boskovic, M. Miljkovic, J. Alloys Compd. 373 (1–2) (2004) 231–236.
[16] K.S. Deepa, S. Nisha, P. Parameswaran, M.T. Sebastian, J. James, Appl. Phys. Lett. 94 (14) (2009) 142902.
[17] J.L. Huang, M.T. Lee, H.H. Lu, D.F. Lii, Mater. Chem. Phys. 45 (3) (1996) 203–210.
[18] J. Liu, Z.J. Shen, M. Nygren, Y.M. Kan, P.L. Wang, J. Eur. Ceram. Soc. 26 (15) (2006) 3233–3239.
[19] Z.J. Shen, H. Peng, J. Liu, M. Nygren, J. Eur. Ceram. Soc. 24 (12) (2004) 3447–3452.
[20] C.H. Lee, H.H. Lu, C.A. Wang, P.K. Nayak, J.L. Huang, J. Am. Ceram. Soc., in press.
[21] B.T. Lee, Y.J. Yoon, K.H. Lee, Mater. Lett. 47 (1–2) (2001) 71–76.
[22] S.T. Buljan, J.G. Baldoni, J. Neil, G. Zilberstein, ORNL/Sub/85-22011/1, GTE, 1988.